

Graphene n - p junction in a strong magnetic field: A semiclassical study

Pierre Carmier,¹ Caio Lewenkopf,² and Denis Ullmo^{1,3}

¹LPTMS UMR 8626, Univ. Paris-Sud, 91405 Orsay Cedex, France

²Instituto de Física, Universidade Federal Fluminense, 24210-346 Niterói, RJ, Brazil

³CNRS, 91405 Orsay Cedex, France

(Received 17 March 2010; revised manuscript received 10 May 2010; published 8 June 2010)

We provide a semiclassical description of the electronic transport through graphene n - p junctions in the quantum Hall regime. A semiclassical approximation for the conductance is derived in terms of the various snakelike trajectories at the interface of the junction. For a symmetric (ambipolar) configuration, the general result can be recovered by means of a simple scattering approach, providing a very transparent qualitative description of the problem under study. Consequences of our findings for the understanding of recent experiments are discussed.

DOI: [10.1103/PhysRevB.81.241406](https://doi.org/10.1103/PhysRevB.81.241406)

PACS number(s): 73.22.Pr, 03.65.Sq, 73.23.Ad, 73.43.Jn

Graphene is a two-dimensional carbon-based material which, due to its remarkable electronic and mechanical properties as well as potential applications, has been the subject of intense research activity in physics, chemistry, and material sciences.^{1,2} At the origin of this interest is the observation that the electronic low-energy dynamics in graphene is governed by a Hamiltonian very similar to that of the two-dimensional relativistic Dirac equation. This has a number of remarkable consequences, two of the most striking being an anomalous quantum Hall effect^{3,4} and the existence of Klein tunneling.⁵⁻⁷

Experiments where both quantum Hall physics in graphene and Klein tunneling are at play were pioneered by Williams *et al.*,⁸ who measured the conductance of graphene n - p junctions in a high magnetic field in the quantum Hall regime. This was possible due to the deposition of a metallic topgate partially covering the graphene sheet. By independently varying the applied top and backgate voltages the resulting electrostatic potential creates negatively and positively doped regions in the graphene sample. In this way n - n , p - p , and n - p junctions were produced. The two former did not show any striking feature. In contrast n - p junctions, where the transition from the electron region to the hole region of the sample has to take place through Klein tunneling, showed a quite unexpected behavior. Conductance plateaus at values $G_0/2$ and $3G_0/4$ ($G_0=2e^2/h$) were observed, at odds with the sequence $(2n+1)G_0$, $n \in \mathbb{Z}$, expected for the quantum Hall effect in graphene. Other experimental groups have observed these and other interesting plateaus in more elaborated setups.⁹⁻¹¹

These observations were explained by Abanin and Levitov¹² through a “quantum chaos hypothesis,” which can be summarized as follows. At the interface between the n and p regions of the junction, the electrons experience a succession of Klein tunneling and skipping-orbit like propagation. It was suggested that the mode mixing caused by this mechanism possibly leads the probability to be transmitted or reflected in a given mode to be perfectly “democratic.” The Landauer-Büttiker formula for the conductance under this hypothesis gives $G=G_0N_nN_p/(N_n+N_p)$, where N_n and N_p are the number of channels in the n and p regions. This simple formula agrees with the observed conductance plateaus.

As already noted,¹² this interpretation fails to provide a

complete explanation of the experimental findings. Indeed, the quantum chaos hypothesis corresponds to the assumption that the scattering matrix describing mode mixing along the junction can be statistically modeled by random-matrix theory. This hypothesis implies that the average scattering matrix coefficients are equal. However, it also predicts universal conductancelike fluctuations,^{13,14} which are quite robust and could not be suppressed by adding disorder.^{15,16} Experiments show reasonably well-defined plateaus, but no significant fluctuation amplitudes around a mean value. An alternative approach^{17,18} showed that the edge boundary conditions affect the valley polarization of the zero-energy Landau level. Clean edges produce new conductance plateaus in the ballistic regime, however, not at the observed values.

The graphene n - p junction plateaus therefore remain an experimental mystery, that we are not going to dispel here. Our goal in this Rapid Communication will be to provide a semiclassical analysis of the mode mixing at the edge of a clean (ballistic) fully coherent n - p junction. In particular, we want to address the question of whether the snakelike motion at the interface can be the microscopic mechanism underlying the quantum chaos hypothesis; we shall see that in spite of what a naive classical intuition would suggest, the answer is essentially negative.

Mode mixing depends on several system-specific features: presence or absence of disorder, steepness of the potential barrier, possible diffractive effects when the electrons transit from their skipping orbit motion along the sample edges to the snakelike motion along the junction interface, etc. To specifically focus on the mixing occurring at the interface, we consider the model sketched in Fig. 1: a perfectly clean graphene sample, the edges of which match smoothly with a steplike potential interface. The Landauer-Büttiker conductance G across the junction is expressed as

$$G = G_0 \sum_{\kappa, \alpha} T_{\kappa, \alpha}, \quad (1)$$

where the sum runs over all the incoming skipping modes κ, α (α is the valley index) in, for instance, the n region and the $T_{\kappa, \alpha}$ are the corresponding transmission probabilities across the junction, for which we present a semiclassical description.

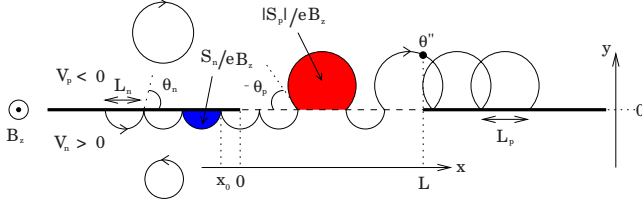


FIG. 1. (Color online) Scattering along a boundary intercalated with a steplike n - p junction. The different symbols are explained in the text.

It is useful to begin by analyzing what are the results expected from a simple classical point of view. Let us call $V_n > 0$ and $V_p < 0$ the electrostatic potential in the n and p regions, respectively (we assume the chemical potential $\mu = 0$), B_z the applied magnetic field, \mathbf{A} the corresponding vector potential, and v_F the Fermi velocity. In the interior of either regions, electrons experience a cyclotron motion of opposite direction and of radius $R_{n,p} = |V_{n,p}| / (eB_z v_F)$. At the sample edge, the classical trajectories follow the skipping motion illustrated in Fig. 1 and can be characterized by the angle at which they hit the boundary.

We call this angle θ_n for trajectories in the n region, and $\pi - \theta_p$ for trajectories in the p region [as it turns out to be more convenient to label the direction of $\mathbf{\Pi} = \mathbf{p} + e\mathbf{A}(\mathbf{r})$, which is antiparallel to the velocity in the hole region]. Between two successive bounces, trajectories progress a distance $L_{n,p} = 2R_{n,p} \sin \theta_{n,p}$ along the edge. The motion is similar at the n - p interface, except that at each encounter with the potential barrier there is a probability

$$\mathcal{T} = \frac{\sin \theta_n \sin \theta_p}{\cos^2\left(\frac{\theta_n - \theta_p}{2}\right)} \quad (2)$$

to be transmitted from the electron side to the hole side (or reciprocally) between two trajectories fulfilling the Snell-Descartes relation

$$R_n \cos \theta_n = R_p \cos \theta_p. \quad (3)$$

Let us consider an incoming mode (κ, α) from the n region. Semiclassically, the mode is built on a one-parameter family of skipping trajectories corresponding to some fixed $\theta_n^{\kappa, \alpha}$. The different trajectories within the family are labeled by the abscissa $x_0 \in [-L_n(\theta_n^{\kappa, \alpha}), 0]$ at which they last bounce before entering the interface region. The evolution of this set of trajectories under the above classical dynamics can be characterized by the probabilities $u_n(x)$ and $u_p(x)$ to emerge at x on the electron side (with angle $\theta_n^{\kappa, \alpha}$) or on the hole side [with the corresponding angle given by Eq. (3)]. If the width L of the junction is significantly larger than L_n and L_p , it can be shown that $u_n(x)$ and $u_p(x)$ converge both toward 1/2 exponentially quickly with the number of bounces on the junction. As a consequence, since whether a trajectory is transmitted or reflected only depends on the side it emerges from after the last scattering at the interface, the classical probability of transmission is, for a large junction, given by the ratio $L_p / (L_n + L_p)$. It should be stressed that this classical transmis-

sion probability, even if averaged on the angle $\theta_n^{\kappa, \alpha}$ specifying the incoming mode, does not correspond to what a quantum chaos hypothesis would require, namely, a probability given by the proportion of available classical phase space on each side of the junction.

Let us now turn to the description of the quantum transmission. For the sake of definitiveness we discuss the case of infinite mass boundary at the edge of the graphene sample. We expect no qualitative differences for either armchair or zigzag boundary conditions. Let us introduce the actions

$$S_n(\theta_n) = eB_z R_n^2 \left(\theta_n - \frac{\sin 2\theta_n}{2} \right), \quad (4)$$

$$S_p(\theta_p) = -eB_z R_p^2 \left(\pi - \theta_p + \frac{\sin 2\theta_p}{2} \right). \quad (5)$$

Semiclassically, the edge modes in the n region are built, within the leads, on the skipping trajectories bouncing on the boundary with an angle $\theta_{\kappa, \alpha}^i$ fulfilling the quantization condition

$$S_n(\theta_n^{\kappa, \alpha}) = 2\pi\hbar(\kappa - \alpha/4) \quad (6)$$

(again, $\alpha = \pm 1$ is the valley index). Note there is no $\kappa = 0$ level for $\alpha = +1$.

We start our semiclassical discussion with the particularly simple case of ambipolar junctions, namely, junctions such that $V_p = -V_n$. In that situation, the Snell relation [Eq. (3)] tells us that $\theta_n = \theta_p$ for any pair of angles, and therefore, $L_n(\theta_n) = L_p(\theta_p)$. As a consequence, the different trajectories within the family $\{\theta_n = \theta_n^{\kappa, \alpha}, x_0 \in [-L_n(\theta_n^{\kappa, \alpha}), 0]\}$ follow a completely independent history. The propagation of the corresponding amplitudes along the junction can be performed for each of them separately and is obtained from the successive multiplications of two 2×2 unitary matrices. The first one,

$$P = \begin{pmatrix} e^{(i/\hbar)S_n(\theta_n) - i(\pi/2) + i\xi} & 0 \\ 0 & e^{(i/\hbar)S_p(\theta_p) + i(\pi/2) + i\xi} \end{pmatrix} \quad (7)$$

with here $\theta_n = \theta_p = \theta_n^{\kappa, \alpha}$, describes the propagation on the electron and hole sides between two interactions with the interface. The $\pm \pi/2$ are the Maslov phases originating from the focal point met on these pieces of trajectory, and $\xi = -\theta_n$ is a Berry phase. The second matrix describes the transmission and reflection between electron and hole sides. It can be expressed as (in a form not restricted to the ambipolar case)

$$D = \begin{pmatrix} r_n e^{i\theta_n} & t_p e^{i(\theta_n + \theta_p)/2} \\ t_n e^{i(\theta_p + \theta_n)/2} & r_p e^{i\theta_p} \end{pmatrix} \quad (8)$$

with $r_n = r_p = -\cos[(\theta_n + \theta_p)/2] / \cos[(\theta_n - \theta_p)/2]$ and $t_{n,p} = -i \sin \theta_{n,p} / \cos[(\theta_n - \theta_p)/2]$. Note the phases $e^{i(\theta_n + \theta_p)/2}$ can be interpreted also as Berry phases. The transmission probability for a given trajectory is then given by $T(\theta_n^{\kappa, \alpha}, x_0) = |(0, 1)(PD)^N(1, 0)^T|^2$ with N the integer part of $(L + |x_0|) / L_n$, which therefore depends on x_0 . The total transmission for the mode (κ, α) is then obtained as $T_{\kappa, \alpha} = L_n^{-1} \int_{-L_n}^0 dx_0 T(\theta_n^{\kappa, \alpha}, x_0)$. The resulting conductance after summation on the modes (κ, α) is shown in Fig. 2.

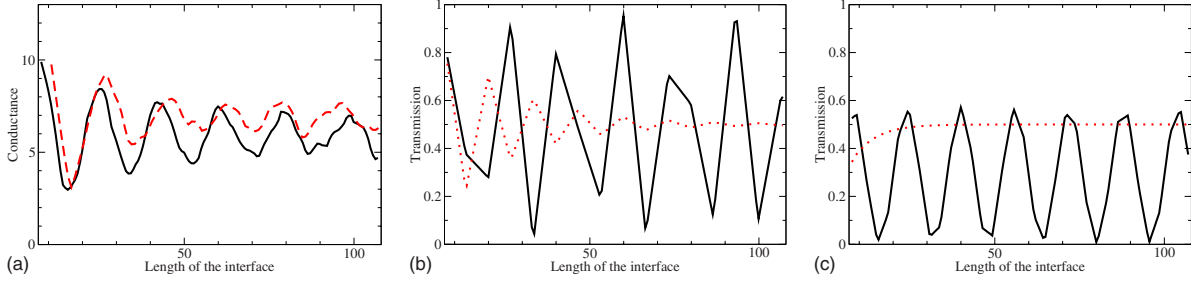


FIG. 2. (Color online) Left: conductance (in units of G_0) as a function of the length of the interface L [in units of the magnetic length $l_B = \sqrt{\hbar/(eB_z)}$] for the case of 13 edge channels (filling factor 7) in the ambipolar (thick black line) and generic (red dashed line) cases. Evidently, no plateau in the conductance is reached in either cases. Middle and right: transmission of edge channels number 4 and 13, for which the local-transmission probability in Eq. (2) is, respectively, $T_4=0.87$ and $T_{13}=0.19$, for semiclassical (thick black line) and classical (red dotted line) dynamics. Substantial difference between both behaviors indicates strong influence of interferences between classical trajectories.

In the generic case of arbitrary V_n and V_p , a semiclassical expression for the conductance can be derived from the Fisher-Lee-Baranger-Stone equations^{19,20} relating the transmission and reflection coefficients $T_{\kappa,\alpha}$ and $R_{\kappa,\alpha}$ to the Green's function $\mathcal{G}(\mathbf{r}'', \mathbf{r}')$ and the incoming mode $\chi_{\kappa,\alpha}^-(\mathbf{r}')$. In our case the transmission can be written as

$$T_{\kappa,\alpha} = \int_{y''>0} dy'' t_{\kappa,\alpha}^\dagger(\mathbf{r}'') v_F \sigma_x t_{\kappa,\alpha}(\mathbf{r}'') \quad (9)$$

with

$$t_{\kappa,\alpha}(\mathbf{r}'') = -i\hbar \int_{y'<0} dy' \mathcal{G}(\mathbf{r}'', \mathbf{r}') v_F \sigma_x \chi_{\kappa,\alpha}^-(\mathbf{r}'). \quad (10)$$

The same results holds for $R_{\kappa,\alpha}$ except that the integral on y'' should be taken for negative values of y'' (i.e., in the electron region). The incoming mode is semiclassically expressed as

$$\chi_{\kappa,\alpha}^-(\mathbf{r}) = \frac{A_{\kappa,\alpha} e^{ik_x^\kappa x}}{\sqrt{|\sin \theta(y)|}} \sum_{\nu=\pm 1} e^{(i/\hbar)\nu S_{\kappa,\alpha}(y) - i\nu(\pi/4)} \begin{pmatrix} e^{-i(\nu/2)\theta(y)} \\ e^{i(\nu/2)\theta(y)} \end{pmatrix} \quad (11)$$

with $\theta(y)$ the angle (>0) such that $y=R_n[\cos \theta_n^{\kappa,\alpha} - \cos \theta(y)]$, $S_{\kappa,\alpha}(y) \equiv (eB_z R_n^2/2)\{\theta(y) - \sin[2\theta(y)]/2\}$, and the normalization coefficient $A_{\kappa,\alpha} = (4v_F R_n \sin \theta_n^{\kappa,\alpha})^{-1/2}$. For the Green's function we take the semiclassical approximation derived in Ref. 21 for the graphene Hamiltonian, properly modified to account for Klein tunneling at the junction interface. The semiclassical Green's function is expressed as a sum over all trajectories j joining \mathbf{r}' to \mathbf{r}''

$$\mathcal{G}_{sc}(\mathbf{r}'', \mathbf{r}'; E) = \frac{1}{i\hbar \sqrt{2\pi i\hbar}} \sum_j \left(\prod_{\xi=n,p} \prod_{\gamma_\xi, \eta_\xi} r_\xi^{\gamma_\xi} t_\xi^{\eta_\xi} \right) \times \frac{e^{(i/\hbar)S_j(\mathbf{r}'', \mathbf{r}') - i(\pi/2)\mu_j + i\xi_j}}{\sqrt{|J_j(\mathbf{r}'', \mathbf{r}')|}} V_j^\epsilon(\mathbf{r}'') V_j^{\epsilon(\mathbf{r}')\dagger}(\mathbf{r}'), \quad (12)$$

where S_j is the action integral along the orbit j , J_j the stability determinant, μ_j the Maslov index counting the focal points met by the trajectory (counted negatively on the hole side), ξ_j is a Berry phase equal to half of the angle of rotation

of the vector $\mathbf{\Pi} = \mathbf{p} + e\mathbf{A}(\mathbf{r})$ (which is parallel to the velocity on the electron side and antiparallel to it on the hole side), $V^+ = \frac{1}{\sqrt{2}} \begin{pmatrix} 1 \\ e^{i\theta} \end{pmatrix}$, $V^- = \frac{1}{\sqrt{2}} \begin{pmatrix} e^{-i\theta} \\ -1 \end{pmatrix}$ with θ the direction of $\mathbf{\Pi}$, and $\epsilon(\mathbf{r}) = +1$ or -1 depending on whether \mathbf{r} is on the electron or the hole side. The only difference introduced by the presence of the potential barrier²² is that bounces on the interface, indexed by $\gamma_{n,p}$, as well as transmission across it, indexed by $\eta_{n,p}$, are taken into account through the coefficients $r_{n,p}$ and $t_{n,p}$ introduced in Eq. (8) (in the definition of which the angles $\theta^{\gamma_{n,p}, \eta_{n,p}}$ are used).

A typical skipping orbit fulfilling the quantization condition Eq. (6) is displayed in Fig. 1. The orbit is characterized by the angle θ' at which it arrives at the Poincaré section $x=L$, the number of excursions m_p on the hole side, and the number of traversals k of the interface. The number of excursions on the electron side is then $m_n(m_p, \theta') = [(W-L' - 2m_p R_p \sin \theta_p)/(2R_n \sin \theta_n)]$ with $[\cdot]$ the integer part and $L' = R_p(\sin \theta_p - \sin \theta')$ for transmission and $R_n(\sin \theta_n + \sin \theta')$ for reflection. The trajectory should also be characterized by the ordering of the various excursions in the n and p sides of the junction. However these various orderings will correspond to the same amplitude, and therefore just contribute as a degeneracy factor given by $\Omega(m_p, k=2k') = \binom{m_p-1}{k'-1} \binom{m_n(m_p)+1}{k'}$ for reflection, and $\Omega(m_p, k=2k'+1) = \binom{m_p}{k'}$ for transmission. Performing the integral in Eq. (10) in the stationary-phase approximation, we get

$$T_{\kappa,\alpha} = \frac{R_p}{2R_n \sin \theta_n^{\kappa,\alpha}} \int_{-\theta_T}^{\theta_T} d\theta' \cos \theta' T_{\kappa,\alpha}(\theta'), \quad (13)$$

$$R_{\kappa,\alpha} = \frac{1}{2 \sin \theta_n^{\kappa,\alpha}} \int_{-\theta_R}^{\theta_R} d\theta' \cos \theta' R_{\kappa,\alpha}(\theta') \quad (14)$$

with

$$T_{\kappa,\alpha}(\theta') = \left| t_n \sum_{m_p=0}^{M_p(\theta')} (-i r_n e^{(i/\hbar)S_n(\theta_n^{\kappa,\alpha})} m_n(m_p, \theta')) \right. \\ \left. \times (i r_p e^{(i/\hbar)S_p(\theta_p)})^{m_p} \sum_{k'} \left(\frac{t_n t_p}{r_n r_p} \right)^{k'} \Omega(m_p, 2k'+1) \right|^2, \quad (15)$$

$$\mathcal{R}_{\kappa,\alpha}(\theta') = \left| \sum_{m_p=0}^{M_p(\theta')} (-ir_n e^{(i/\hbar)S_n(\theta_n^{\kappa,\alpha})} m_n(m_p, \theta') + 1) \times (ir_p e^{(i/\hbar)S_p(\theta_p)})^{m_p} \sum_{k'} \left(\frac{t_n t_p}{r_n r_p} \right)^{k'} \Omega(m_p, 2k') \right|^2, \quad (16)$$

where $M_p(\theta') = [(W-L')/(2R_p \sin \theta_p)]$, $\theta_T = \min(\theta_p, \pi - \theta_p)$, and $\theta_R = \min(\theta_n^{\kappa,\alpha}, \pi - \theta_n^{\kappa,\alpha})$. The corresponding curves for the conductance in Eq. (1) are shown in Fig. 2.

A few comments are in order. First, we stress that in the ambipolar case $V_p = -V_n$, the results obtained within the Baranger-Stone framework are, as expected, strictly identical to those derived earlier with the “scattering matrix” approach. Second, the equilibration and thus the saturation of the conductance expected at the classical level has to be contrasted with the persisting large oscillations of the semiclassical conductance. Finally and more surprisingly, we observe that the mean of the semiclassical prediction can differ significantly from the classical limiting value. This is illustrated, for instance, at the rightmost panel of Fig. 2.

Understanding the oscillating pattern in the conductance as a function of the length of the interface in Fig. 2 is relatively straightforward in the ambipolar case, since the “scattering matrix” can be interpreted as that of a rotation on the Bloch sphere, acting on the vector composed of reflection and transmission probability amplitudes of a given mode. In particular convergence to a given transmission probability, corresponding to a vector pointing at a fixed latitude, cannot be achieved. Outside of the ambipolar case, this interpretation is no longer valid but the pattern of the conductance in Fig. 2 is similar enough to let us believe this picture remains qualitatively correct.

The advantage of a semiclassical description, compared,

for instance, to an exact numerical calculation of the conductance using recursive Green’s function techniques, is that it makes it possible to discuss the expected consequence of various modifications of the model we consider. For instance, we do not expect that including a finite width d_w in the potential step (as long as $d_w \ll l_B$) or changing the edge-boundary conditions will qualitatively modify the oscillating pattern of the conductance. In the first case, the local probability transmission Eq. (2) will be somewhat smaller, actually improving the speed of classical convergence. In the second case, the quantization condition in Eq. (6) will be modified,²³ but without affecting the basic mechanism at play here. A geometry closer to the one used in experiments, i.e., with the junction perpendicular to the edge of the ribbon, would imply some diffraction at the edge-junction corner (this aspect will be discussed in more details in Ref. 24). This, as more generally the inclusion of a weak disorder, would somewhat diminish the amplitude of the conductance oscillations and bring the average of the semiclassical results closer to the classical conductance.

As increasing the amount of disorder could only bring the system toward a chaotic limit, characterized by universal conductance fluctuations around a mean given by the classical (democratic) expectation, our study indicates that within a model of perfectly coherent electrons, the intrinsic properties of the n - p junction cannot produce the experimentally observed plateaus. These considerations suggest the existence of inelastic processes occurring in the vicinity of the junction, possibly reducing the coherence length ℓ_ϕ to values smaller than L . Further experiments, varying the ratio ℓ_ϕ/L , are expected to provide further insight on this issue.

We acknowledge a fruitful discussion with Alfredo Ozorio de Almeida. This research was supported by the CAPES/COFECUB (project Ph 606/08).

¹A. H. Castro Neto, F. Guinea, N. M. R. Peres, K. S. Novoselov, and A. K. Geim, *Rev. Mod. Phys.* **81**, 109 (2009).

²A. K. Geim, *Science* **324**, 1530 (2009).

³K. S. Novoselov, A. K. Geim, S. V. Morozov, D. Jiang, M. I. Katsnelson, I. V. Grigorieva, S. V. Dubonos, and A. A. Firsov, *Nature (London)* **438**, 197 (2005).

⁴Y. Zhang, Y. W. Tan, H. L. Stormer, and P. Kim, *Nature (London)* **438**, 201 (2005).

⁵M. I. Katsnelson, K. S. Novoselov, and A. K. Geim, *Nat. Phys.* **2**, 620 (2006).

⁶A. F. Young and P. Kim, *Nat. Phys.* **5**, 222 (2009).

⁷N. Stander, B. Huard, and D. Goldhaber-Gordon, *Phys. Rev. Lett.* **102**, 026807 (2009).

⁸J. R. Williams, L. DiCarlo, and C. M. Marcus, *Science* **317**, 638 (2007).

⁹B. Özyilmaz, P. Jarillo-Herrero, D. Efetov, D. A. Abanin, L. S. Levitov, and P. Kim, *Phys. Rev. Lett.* **99**, 166804 (2007).

¹⁰D.-K. Ki and H.-J. Lee, *Phys. Rev. B* **79**, 195327 (2009).

¹¹T. Lohmann, K. von Klitzing, and J. H. Smet, *Nano Lett.* **9**, 1973 (2009).

¹²D. A. Abanin and L. S. Levitov, *Science* **317**, 641 (2007).

¹³H. U. Baranger and P. A. Mello, *Phys. Rev. Lett.* **73**, 142 (1994).

¹⁴R. A. Jalabert, J.-L. Pichard, and C. W. J. Beenakker, *Europhys. Lett.* **27**, 255 (1994).

¹⁵W. Long, Q. F. Sun, and J. Wang, *Phys. Rev. Lett.* **101**, 166806 (2008).

¹⁶J. Li and S. Q. Shen, *Phys. Rev. B* **78**, 205308 (2008).

¹⁷J. Tworzydło, I. Snyman, A. R. Akhmerov, and C. W. J. Beenakker, *Phys. Rev. B* **76**, 035411 (2007).

¹⁸A. R. Akhmerov, J. H. Bardarson, A. Rycerz, and C. W. J. Beenakker, *Phys. Rev. B* **77**, 205416 (2008).

¹⁹D. S. Fisher and P. A. Lee, *Phys. Rev. B* **23**, 6851 (1981).

²⁰H. U. Baranger and A. D. Stone, *Phys. Rev. B* **40**, 8169 (1989).

²¹P. Carmier and D. Ullmo, *Phys. Rev. B* **77**, 245413 (2008).

²²L. Couchman, E. Ott, and T. M. Antonsen, *Phys. Rev. A* **46**, 6193 (1992).

²³P. Rakyta, A. Kormanyos, J. Cserti, and P. Koskinen, *Phys. Rev. B* **81**, 115411 (2010).

²⁴P. Carmier, C. Lewenkopf, and D. Ullmo (unpublished).